Structural Control & Health Monitoring, accepted: 16/10/2019

AN INERTER-EQUIPPED VIBRATING BARRIER FOR NON-INVASIVE MOTION CONTROL OF SEISMICALLY EXCITED STRUCTURES

Pierfrancesco CACCIOLA[1], Alessandro TOMBARI[1], Agathoklis GIARALIS[2]

1 School of Environment and Technology, University of Brighton, Brighton, UK
2 Department of Civil Engineering, City, University of London, London, UK

ABSTRACT

The Vibrating Barrier (ViBa) is a large-scale oscillating mass-spring-damper unit contained in the ground and tuned to mitigate the motion of surrounding structures under earthquake-induced ground shaking, without being directly in contact to them, through a structure-soil-structure interaction mechanism. Previous research showed that ViBa achieves significant seismic structural response reductions but, in doing so, it requires excessive vibrating mass, equal to the mass of the structure that aims to control or more, which hinders its practical applicability. This paper considers coupling ViBa with a grounded inerter acting as a mass amplifier to reduce ViBa mass/weight in suppressing seismically induced structural response. Attention is focused on structures amenable to modelling as single-degree-of freedom (SDOF) damped oscillators by establishing equations of motion of a 5-DOF dynamical system of a grounded inerter-equipped ViBa (IViBa) fused with a SDOF structure and accounting for soil structure interaction (SSI) effects due to soil compliance. Optimal closed-form H_∞ and numerical H_2 IViBa tuning are addressed minimizing the response of SDOF structure subject to harmonic resonant and to broadband/white base excitation, respectively. Numerical results pertaining to a small-scale physical ViBa prototype specimen are furnished quantifying the trade-off between IViBa mass and inertance considering non-rigid/compliant inerter-to-ground connectivity. Monotonic IViBa mass/weight reduction trend is found for fixed targeted structural performance under white stationary as well as colored non-stationary seismic excitation for increasing inertance and for sufficiently rigid inerter-to-ground connection. It is concluded that careful engineering design of the inerter-to-ground connection minimizing compliance is most critical in fully exploiting the beneficial effects of grounded inerter for mass/weight IViBa reduction facilitating, thus, its practical implementation.

Keywords: Vibrating Barrier; inerter; structure-soil-structure interaction; optimal design, non-stationary excitation

1. INTRODUCTION

New building structures in seismically prone areas can be readily designed to achieve acceptable level of seismic performance through code-prescriptive capacity/ductile design for earthquake resistance (e.g., Avramidis et al. [1]) and/or through equipping them with energy dissipation devices including viscous, viscoelastic, and hysteretic dampers (e.g., Soong and Dargush [2]) as well as with tuned mass dampers (TMDs) (e.g., De Angelis et al. [3], Matta [4]). Alternatively, the same can be achieved through seismic isolation making use of laterally flexible bearings at the interface of the structure and its foundation which decouple the motion of the building from the earthquake-induced ground motion (e.g., Naeim and Kelly [5]). Nevertheless, seismic protection of existing code-deficient buildings is an appreciably more involved task requiring invasive and expensive interventions to seismically upgrade structural performance through increased stiffness, strength, and/or ductility (Fardis [6]) or through equipping structures with energy dissipation devices or a base isolation layer. In practice, building owners can rarely afford the cost of such interventions leaving much of the existing building stock in major cities vulnerable to future seismic events (e.g., Kappos and

Dimitrakopoulos [7]). Moreover, in case of heritage structures most types of structural intervention for seismic upgrade applicable to ordinary structures are not allowed as they would compromise their architectural/historical value.

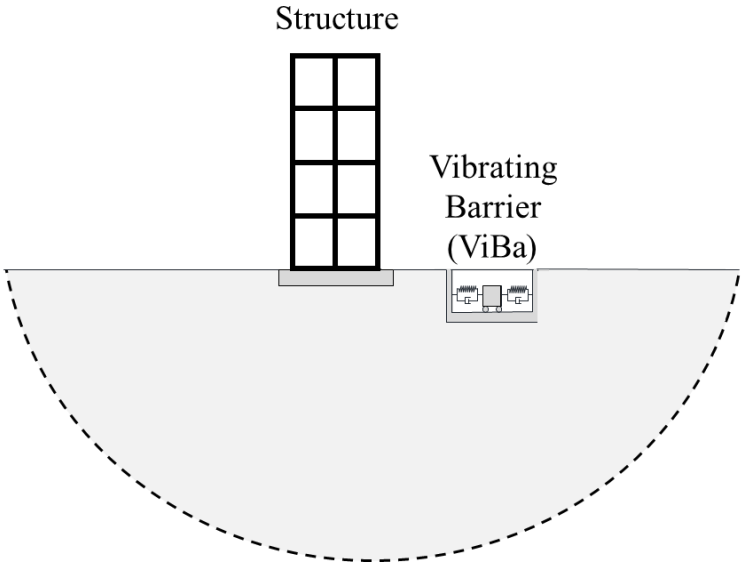

Figure 1. Schematic depiction of a vibrating barrier protecting an existing structure from earthquake-induced ground motion.

To this end, a viable way to address the above economically non-feasible for private building owners or non-applicable for heritage structures invasive solutions for seismic protection of existing structures is to modify/control their seismic response by changing their surrounding/support ground field. Along these lines, in an early work, Woods [8] demonstrated, through a field investigation, the potential of excavating open trenches to the ground surrounding a given structure to mitigate seismic structural response due to Rayleigh seismic surface waves. More recently, several researchers explored the concept of embedding to the ground around structures multiple oscillating units of significant mass judicially distributed and positioned to filter out incoming seismic waves within a certain frequency band in which resonant structural frequencies lie (see e.g., Krodel et al. [9], Dertimanis et al. [10], Palermo et al. [11] and reference therein). In this manner, these metamaterial-like structures act as shields/barriers for seismic waves of significant structural damage potential, whose design is based on seismic wave propagation principles and elasto-dynamic considerations. Nevertheless, all the above reviewed approaches for non-invasive seismic protection of structures address only surface seismic waves and cannot control structural response due to body seismic waves which may be significant especially in near-fault conditions. To this end, an alternative, considerable different, approach has been recently proposed by the first two authors (Cacciola and Tombari [12]), termed Vibrating Barrier (ViBa), to suppress the motion of seismically excited structures irrespective of the nature of the seismic waves. This is achieved by relying on discrete passive vibration control principles, rather than elasto-dynamics, aiming to dissipate seismic kinetic energy rather than reflecting or refracting the various types of seismic waves. Specifically, ViBa comprises a free-to-vibrate mass encased in a rigid containment buried in the ground and connected to the walls of the containment through linear springs and dampers as depicted in Figure 1. It can therefore be viewed as an underground TMD-like unit tuned to absorb portion of the seismic energy before entering the foundations of surrounding structures by exploiting a structure-soil-structure (SSSI) mechanism. The latter involves the dynamic interaction between two (or more) adjacent rigid structures resting on relatively soft/compliant soil media (e.g., Warburton et al. [13]). In fact,

SSSI has been heavily studied in the literature to explain differences in seismic response of structures located away from any other structure as opposed to being near other structures (see e.g., Lou et al. [14] and references therein). To date, several studies on the efficiency of the ViBa have been carried out to mitigate the seismic vulnerability of different structures. Cacciola et al. [15] investigated the potential of ViBa for the seismic protection of monopiled structures, Tombari et al. [16] considered ViBa to mitigate seismic risk of a nuclear reactor, Cacciola et al. [17] applied ViBa to control the seismic response of a heritage building, while the ViBa technology was used to protect a large urban area in Coronado et al. [18], as well as a cluster of buildings in Tombari et al. [19]. All the above studies have collectively demonstrated remarkable effectiveness of ViBa in reducing peak structural response which, in the case of narrow-band/harmonic excitations, can be higher than 60%, while for broadband/earthquake excitations reaches more than 30%.

Nevertheless, the effectiveness of ViBa in containing structural seismic response demands depends largely on its inertial property: the higher the ViBa mass is, the more dramatic the reductions in peak structural response becomes which is similar to the case of TMDs used for the seismic protection of building structures (e.g. [3]). In this regard, the above reported reductions to seismic response require ViBa mass/weight as large as the total mass of the structure to be protected which needs to be embedded to the ground. This requirement results in significant excavation, underground space usage, and construction costs which hinders the applicability of ViBa in real-life applications. To address the above major limitation of ViBa (i.e., required excessive mass), this paper considers incorporating an inerter, defined as a two-terminal mechanical element developing a resisting force proportional to the relative acceleration of its terminals (Smith [20]), to connect the ViBa mass to the ground. In this arrangement, the inerter acts potentially as an inertial/mass amplifier. This is because it develops a resisting force proportional to the relative to the ground ViBa mass acceleration and to the inerter constant of proportionality, termed inertance, and measured in mass (kg) units (see also [20]). In the meantime, the inertance is independent of the mass/weight of inerter devices. Indeed, inerter device prototypes have been manufactured and verified experimentally attaining inertance several orders of magnitude larger than their physical mass (e.g. Papageorgiou and Smith [21]) reaching inertance of more than 12000tons as required in earthquake engineering applications [22]. In this junction, it is important to note that the mass amplification effect of a rigidly grounded inerter was shown to enhance vibration suppression performance in TMD-equipped structures subject to white noise (Marian and Giaralis [23]), sinusoidal (Marian and Giaralis [24]), and earthquake-induced (Pietrosanti et al. [25]) base excitations. Further, Lazar et al. [26] and Giaralis and Taflanidis [27] demonstrated that inerter-equipped TMDs are quite effective for seismic response reduction of multi-storey building structures when placed in the ground floor with the inerter rigidly connected to the ground. Along similar lines, De Domenico and Ricciardi [28] demonstrated the enhanced effectiveness of coupling a TMD with a grounded inerter for seismic protection of base-isolated buildings. To a large extent, the herein newly proposed grounded inerter-equipped ViBa, hereafter IViBa, is motivated by the above referenced works on inerter-equipped TMDs.

In this study, the potential of IViBa for seismic vibration mitigation is investigated for the case of a single structure whose seismic response can be faithfully represented by a single-degree-of freedom (SDOF) damped oscillator. To this aim, a novel 5-DOF dynamical system of the proposed IViBa fused with a SDOF structure and accounting for soil structure interaction (SSI) effects due to soil compliance is introduced and its equations of motion are derived. The adopted system enables to study parametrically the effects of different IViBa inertial properties, i.e., mass and inertance, as well as the level of inerter-to-ground level of rigidity to the effectiveness of IViBa to mitigate the SDOF structure response to different types of seismic

excitation. Optimal closed-form H_∞ and numerical H_2 IViBa tuning are considered minimizing the response of SDOF structure subject to harmonic resonant and to broadband/white base excitation, respectively. In the numerical part of the work, the properties of a small-scale physical specimen of a ViBa coupled with a SDOF oscillator structure with SSI and SSSI effects considered by Cacciola and Tombari [12] is adopted as case-study. Attention is focused on comparing the performance of IViBa with the same inertia contributed by a different combination of mass and inertance as well as quantifying the influence of the inertance and of the inerter-to-ground connection rigidity to IViBa mass/weight reduction for fixed structural seismic performance under different types of seismic excitation.

2. Proposed inerter-equipped vibrating barrier (IViBa)

2.1 Mechanical model description

The planar discrete mechanical model shown in Figure 2 is herein put forward to examine the potential of an IViBa for the seismic protection of a single building through the SSSI mechanism as numerically and experimentally established in [12] for the ViBa (Figure 1). In the adopted model, the building is represented by a linear viscously damped single-degree-of-freedom (SDOF) system with stiffness k, damping coefficient c, and mass m, resting on compliant soil. Soil-structure interaction (SSI) effect to building response due to soil compliance of the supporting ground is accounted for through the stiffness, k_f, damping coefficient, c_f, and lumped foundation mass, m_f. Further, the IViBa, encircled by a red box with broken line in Figure 2, is represented by a linear SDOF oscillating unit with lumped mass, m_{IViBa}, spring stiffness, k_{IViBa}, and damping coefficient, c_{IViBa}, housed in a containment with lumped

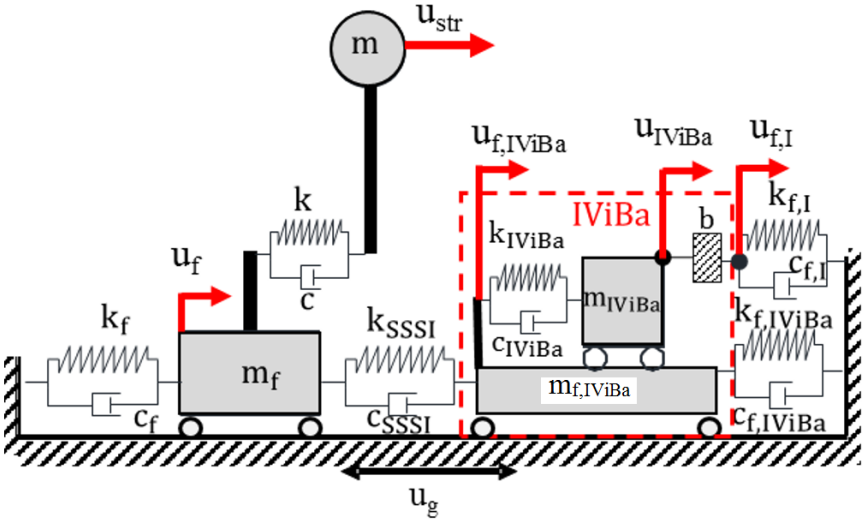

Figure 2. Mechanical model of an IViBa coupled with a linear SDOF structure.

mass $m_{f,IViBa}$. An inerter element with inertance b connects the IViBa oscillating unit to the ground. The SSI effects associated with the IViBa container are modelled through the stiffness coefficient, $k_{f,IViBa}$ and the damping coefficient $c_{f,IViBa}$. Further, soil compliance at the connection of the inerter to the ground is accounted for by means of the stiffness, $k_{f,I}$, and damping coefficient, $c_{f,I}$. The latter consideration is dictated by the large force expected to develop by the inerter and be transmitted to the ground during severe earthquake excitations as discussed in Makris and Kampas [29]. Lastly, the SSSI mechanism is captured by a linear elastic spring with k_{SSSI} stiffness constant and a dashpot with c_{SSSI} damping coefficient linking the foundation of the SDOF system to the IViBa containment following the work of Mulliken and Karabalis [30]. It is noted that the system in Figure 2 is a simplification of the more

complex real case scenario in which the multicomponent incoming surface and body waves might be different underneath both the structure and the ViBa. In Cacciola and Tombari [12] and Tombari et al. [19] the simplified lumped parameter model, herein extended to include the inerter device, has been compared with more advanced FEM/BEM numerical models accounting for seismic wave propagation following a vertical path from the bedrock and potential modification of the seismic excitation. In those papers it has been proved that simplified model provides accurate results suitable for the design of the Vibrating Barrier. Various procedures can be used to determine the reduced model for the design of the Vibrating Barrier such as those proposed by Tombari et al. [19] exploiting the Craig-Bampton approach or those proposed by Casciati and Faravelli [31] including nonlinear component".

Compared to the original ViBa configuration and its underlying dynamical model introduced in [12], the key additional component furnished by the IViBa is the inerter element with one terminal grounded. In the IViBa configuration, the overall inertial (i.e., acceleration dependent) force developed by the IViBa under a horizontal ground displacement, u_g, as shown in Figure 2 is given as

$$F_I = F_m + F_b = m_{IViBa}\ddot{u}_{IViBa} + b\left(\ddot{u}_{IViBa} - \ddot{u}_{f,I}\right), \quad (1)$$

where u_{IViBa} is the total (absolute) displacement of the IViBa oscillating unit, $u_{f,I}$ is the total displacement of the inerter connection to the ground and hereafter a dot over a symbol denotes differentiation with respect to time. Therefore, the inclusion of the grounded inerter contributes to the mass-related inertial force, $F_m = m_{IViBa}\ddot{u}_{IViBa}$, of the conventional ViBa an additional inerter-related inertial force, $F_b = b\left(\ddot{u}_{IViBa} - \ddot{u}_{f,I}\right)$, proportional to the relative acceleration of the inerter terminals following the definition of the inerter element [20]. Clearly, the significance of the contributed inerter force to the overall inertial IViBa force and, ultimately, to the potential of IViBa to control the response of the SDOF structure depends on the inertance value b as well as on the term $\left(\ddot{u}_{IViBa} - \ddot{u}_{f,I}\right)$. The latter, in turn, depends on the level of soil compliance or, equivalently, on the level of rigidity of the inerter-to-ground connection which influences the term $\ddot{u}_{f,I}$ (e.g., note that for perfectly rigid connection $\ddot{u}_{f,I} = \ddot{u}_g$, that is, the ground acceleration). Later, in Section 4, the influence of both the above discussed factors (i.e., inertance and soil compliance) to the vibration suppression potential of the IViBa is parametrically investigated in order to compare and highlight differences between IViBa from the conventional ViBa for which $b = 0$ and $F_I = F_m$ in Eq.(1). In closing this section, it is important to note that, similarly to the IViBa dashpot in Figure 2 representing one or more viscous dampers in parallel connection, the inerter element in Figure 2 models one or more linear inerter devices arranged in parallel. Further, the inerter element is taken as mass-less independently of the inertance b. This is because the inertance of actual inerter devices can be several orders of magnitude larger than the physical device mass (see e.g., [20], [22], [24]). In this regard, the inertance property of the IViBa can scale-up to values of the same order of m_{IViBa} and, therefore, of m (mass of the existing structure to be controlled).

2.2 Equations of motion and transfer functions

The response of the seismically excited mechanical model in Figure 2 is described by 5 translational degrees-of-freedom (DOFs), as indicated on the same Figure, taken in terms of absolute ordinates/displacements which is the norm in SSI and SSSI studies. These include the displacements of the SDOF structure and its foundation, u_{str} and u_f, respectively, the displacements of the IViBa oscillating unit and its containment, u_{IViBa} and $u_{f,IViBa}$, respectively, and the displacement of the inerter connection to the ground, $u_{f,I}$. The equations of motion of the considered dynamical model in time domain are written in matrix form as

$$\mathbf{M}\ddot{\boldsymbol{u}}(t) + \mathbf{C}\dot{\boldsymbol{u}}(t) + \mathbf{K}\boldsymbol{u}(t) = \mathbf{Q}_{\boldsymbol{e}} u_{\mathrm{g}}(t) + \mathbf{Q}_{\boldsymbol{d}} \dot{u}_{\mathrm{g}}(t), \tag{2}$$

where $\boldsymbol{u}(t)$ is the response displacement vector defined as

$$\boldsymbol{u}(t) = [\mathrm{u_{str}}(t) \quad \mathrm{u_f}(t) \quad \mathrm{u_{f,IViBa}}(t) \quad \mathrm{u_{IViBa}}(t) \quad \mathrm{u_{f,I}}(t)]^T, \tag{3}$$

in which the superscript "T" is the matrix transpose operator; **M**, **C,** and **K** are the mass, stiffness, and damping matrices, respectively, given as

$$\mathbf{M} = \begin{bmatrix} \mathrm{m} & 0 & 0 & 0 & 0 \\ 0 & \mathrm{m_f} & 0 & 0 & 0 \\ 0 & 0 & \mathrm{m_{f,IViBa}} & 0 & 0 \\ 0 & 0 & 0 & \mathrm{m_{IViBa}} + \mathrm{b} & -\mathrm{b} \\ 0 & 0 & 0 & -\mathrm{b} & \mathrm{m_{f,I}} + \mathrm{b} \end{bmatrix}, \tag{4}$$

$$\mathbf{C} = \begin{bmatrix} \mathrm{c} & -\mathrm{c} & 0 & 0 & 0 \\ -\mathrm{c} & \mathrm{c} + \mathrm{c_f} + \mathrm{c_{SSSI}} & -\mathrm{c_{SSSI}} & 0 & 0 \\ 0 & -\mathrm{c_{SSSI}} & \mathrm{c_{IViBa}} + \mathrm{c_{f,IViBa}} + \mathrm{c_{SSSI}} & -\mathrm{c_{IViBa}} & 0 \\ 0 & 0 & -\mathrm{c_{IViBa}} & \mathrm{c_{IViBa}} & 0 \\ 0 & 0 & 0 & 0 & \mathrm{c_{f,I}} \end{bmatrix}, \tag{5}$$

and

$$\mathbf{K} = \begin{bmatrix} \mathrm{k} & -\mathrm{k} & 0 & 0 & 0 \\ -\mathrm{k} & \mathrm{k} + \mathrm{k_f} + \mathrm{k_{SSSI}} & -\mathrm{k_{SSSI}} & 0 & 0 \\ 0 & -\mathrm{k_{SSSI}} & \mathrm{k_{IViBa}} + \mathrm{k_{f,IViBa}} + \mathrm{k_{SSSI}} & -\mathrm{k_{IViBa}} & 0 \\ 0 & 0 & -\mathrm{k_{IViBa}} & \mathrm{k_{IViBa}} & 0 \\ 0 & 0 & 0 & 0 & \mathrm{k_{f,I}} \end{bmatrix}; \tag{6}$$

and the influence vectors $\mathbf{Q}_{\boldsymbol{e}}$ and $\mathbf{Q}_{\boldsymbol{d}}$ are given as

$$\mathbf{Q}_{\boldsymbol{e}} = [0 \quad \mathrm{k_f} \quad \mathrm{k_{f,IViBa}} \quad 0 \quad \mathrm{k_{f,I}}]^T, \tag{7}$$

and

$$\mathbf{Q}_{\boldsymbol{d}} = [0 \quad \mathrm{c_f} \quad \mathrm{c_{f,IViBa}} \quad 0 \quad \mathrm{c_{f,I}}]^T. \tag{8}$$

It is worth emphasising that the mass matrix, **M**, in Eq.(4) collects all lumped masses of the system in its main diagonal but it is non-diagonal due to the inclusion of the inerter.

For the purposes of this work, the solution of the equations of motion in Eq. (1) is pursued in the domain of circular frequencies ω. To this aim, equations of motion in Eq.(1) are first written in frequency domain by application of the Fourier transform as

$$[\mathbf{K} - \omega^2\mathbf{M} + \mathrm{i}\omega\mathbf{C}]\mathbf{U}(\omega) = \mathbf{Q}(\omega)\, \mathrm{U_g}(\omega), \tag{9}$$

where $\mathrm{i} = \sqrt{-1}$; $\mathrm{U_g}(\omega)$ is the Fourier transform of the ground displacement u_{g}; $\mathbf{U}(\omega)$ is the vector collecting the Fourier transformed elements of the response displacement vector in Eq.(3) given as

$$\mathbf{U}(\omega) = [\mathrm{U_{str}}(\omega) \quad \mathrm{U_f}(\omega) \quad \mathrm{U_{f,IViBa}}(\omega) \quad \mathrm{U_{IViBa}}(\omega) \quad \mathrm{U_{f,I}}(\omega)]^T; \tag{10}$$

and **Q** is an influence vector defined as

$$\mathbf{Q}(\omega) = [\mathbf{K} + \mathrm{i}\omega\mathbf{C}]\boldsymbol{\tau} = [0 \quad \mathrm{k_f} + \mathrm{i}\omega\mathrm{c_f} \quad \mathrm{k_{f,IViBa}} + \mathrm{i}\omega\mathrm{c_{f,IViBa}} \quad 0 \quad \mathrm{k_{f,I}} + \mathrm{i}\omega\mathrm{c_{f,I}}]^{\mathrm{T}}, \tag{11}$$

in which $\boldsymbol{\tau}$ is the unitary vector.

Next, Eq.(9) is solved as in

$$\mathbf{U}(\omega) = \mathbf{H}(\omega)\,\mathrm{U_g}(\omega), \tag{12}$$

where

$$\mathbf{H}(\omega) = [\mathbf{K} - \omega^2\mathbf{M} + \mathrm{i}\omega\mathbf{C}]^{-1}\mathbf{Q}(\omega) \tag{13}$$

is a vector collecting the transfer functions relating the displacement response along all the 5 DOFs of the considered model with the ground excitation displacement. That is,

$$\mathbf{H}(\omega) = \left[\mathrm{H_{str}} = \frac{\mathrm{U_{str}}}{\mathrm{U_g}} \quad \mathrm{H_f} = \frac{\mathrm{U_f}}{\mathrm{U_g}} \quad \mathrm{H_{f,IViBa}} = \frac{\mathrm{U_{f,IViBa}}}{\mathrm{U_g}} \quad \mathrm{H_{IViBa}} = \frac{\mathrm{U_{IViBa}}}{\mathrm{U_g}} \quad \mathrm{H_{f,I}} = \frac{\mathrm{U_{f,I}}}{\mathrm{U_g}}\right]^{\mathrm{T}} \tag{14}$$

in which the dependency of all terms appearing on the circular frequency ω has been omitted.

The first element of the transfer function vector in Eq. (14), i.e., the transfer function $\mathrm{H_{str}}(\omega)$ corresponding to the SDOF system displacement, forms the basis for optimal tuning/designing of the IViBa discussed in the following section. It is reiterated that for $\mathrm{b} = 0$ the DOF corresponding to the $\mathrm{u_{f,I}}$ ordinate is uncoupled from the other DOFs of the mechanical model in Figure 2 and, hence, the equations of motion in Eq. (2) degenerate to those of the original ViBa [12].

3. Optimal design of inerter-equipped vibrating barrier (IViBa)

Having established the equations of motion and transfer function vector of the coupled IViBa with SDOF system, this section discusses optimal IViBa design/tuning for harmonic and for broadband/white ground excitation aiming to suppress the displacement response, $\mathrm{u_{str}}$, of the SDOF system in Figure 2. The section starts with discussing the primary and secondary design variables of choice.

3.1 Design variables

IViBa aims to control seismically induced vibrations in adjacent existing structures. Therefore, the properties of the SDOF system in Figure 2, k, m, and c, are treated as known. Further, foundation, SSI, and SSSI parameters are also taken as known for both the structure and the IViBa unit. They can be determined using standard approaches from soil mechanics and dynamics based on the geometry of the structure foundation and the IViBa containment as well as the site soil properties (e.g., Kramer [32]). Moreover, Cacciola et al. [15] demonstrated that ViBa efficiency for seismic vibrations mitigation increases monotonically with increasing the mass of the ViBa oscillating unit as in the case of standard tuned mass dampers (e.g., [3]). In this regard, the IViBa mass, $\mathrm{m_{IViBa}}$, will attain an *a priori* known value to ensure convexity in the IViBa optimal design problem. Based on the same reasoning, IViBa inertance, b, is also herein treated as *a priori* known since previous studies on tuned inertial/mass dampers incorporating a grounded inerter report monotonically increasing seismic vibration control performance with inertance [23,24,26]. To this end, the next presented optimal IViBa design problem involves determining two design variables, namely IViBa stiffness, $\mathrm{k_{IViBa}}$, and damping coefficient, $\mathrm{c_{IViBa}}$, such that the peak displacement $\mathrm{u_{str}}$ of a given structure subjected to known seismic excitation is minimized for *a priori* fixed IViBa inertial properties: mass, $\mathrm{m_{IViBa}}$, and inertance, b. Conveniently, note that the adopted optimal design formulation allows for explicit treatment of the ViBa as special case by setting $\mathrm{b} = 0$ while facilitates

design and comparison of IViBas with different inertial properties set as desired. This consideration is exploited in the numerical part of this work to explore the potential of inertance in reducing required IViBa mass and, consequently, IViBa weight, volume, and excavation cost, for effective vibration suppression.

3.2 Optimal H_∞ IViBa tuning for harmonic excitation

Consider first the case of harmonic ground excitation in which $U_g(\omega_f) = 1$ in Eq. (12) where ω_f is the circular frequency of the excitation. Minimization of the peak displacement u_{str} of the SDOF structure can be achieved by requiring minimization of the magnitude of the transfer function $H_{str}(\omega)$ in Eq. (14) at $\omega = \omega_f$ through optimal IViBa tuning. The above optimization problem is mathematically expressed as

$$\underset{\boldsymbol{\alpha}}{\mathbf{min}}\{|H_{str}(\omega_f)|\} \text{ where } \boldsymbol{\alpha} = \{k_{IViBa}, c_{IViBa}\} \in \mathbb{R}_0^+ \tag{15}$$

supporting optimal control design in the infinity norm, H_∞, sense (see e.g. Zuo, [33]; Toscano, [34]). Equation (15) is solved in closed-form by finding the zeros of the transfer function $H_{str}(\omega)$ at frequency ω_f, that is, the roots of the numerator of $H_{str}(\omega)$ given as

$$\mathbf{num}\{|H_{str}(\omega_f)|\} = (a_1\mu + a_2)\bar{k}_{IViBa} - (a_3\mu + a_4), \tag{16}$$

where

$$\begin{aligned}
a_1 &= -k_v\left[\bar{k}_{sssi} - \omega_f^2 m_{fv} - k_v + (\kappa+\chi)\left(\bar{k}_{sssi} + \bar{k}_f\right)\right] \\
a_2 &= \kappa\bar{k}_f\left(\bar{k}_{sssi} - k_v + \chi\left(\bar{k}_{sssi} + \bar{k}_f\right) - m_{fv}\omega_f^2\right) \\
a_3 &= \kappa k_v\bar{k}_f\left[\bar{k}_{sssi} + \chi\left(\bar{k}_f + \bar{k}_{sssi}\right) - m_{fv}\omega_f^2\right] - k_v^2\left[\bar{k}_{sssi} + \chi\left(\bar{k}_{sssi} + \bar{k}_f\right) - \omega_f^2 m_{fv}\right] \\
a_4 &= \kappa k_v\bar{k}_f\left[\bar{k}_{sssi} + \chi\left(\bar{k}_f + \bar{k}_{sssi}\right) - m_{fv}\omega_f^2\right]
\end{aligned} \tag{17}$$

In the above expressions, the following dimensionless parameters are used

$$\mu = \frac{b}{m_{IViBa}}, \kappa = \frac{\bar{k}_{f,I}}{\bar{k}_f}, k_v = m_{IViBa}\omega_f^2 \text{ and } \chi = \frac{\bar{k}_{f,IViBa}}{\bar{k}_f}, \tag{18}$$

while $\bar{k}_x$ denotes the complex quantity $k_x + i\omega_f c_x$.

In this setting, the optimization problem in Eq. (15) is solved by determining the complex valued $\bar{k}_{IViBa}$ parameter satisfying the conditions

$$(a_1\mu + a_2)\bar{k}_{IViBa} - (a_3\mu + a_4) = 0\,; \;\; \mathbf{den}\{|H_{str}(\omega_f)|\} \neq 0, \tag{19}$$

in which it is understood that the condition on the denominator is only applicable to the special case of an undamped system, since the presence of damping, as is assumed throughout the numerical part of this work, ensures that the condition is always satisfied. After some algebra, the following expression for $\bar{k}_{IViBa}$ is reached

$$\bar{k}_{IViBa} = \frac{k_v[\mu k_v - \kappa\bar{k}_f(\mu+1)]\left[\bar{k}_{sssi} + \chi\left(\bar{k}_f + \bar{k}_{sssi}\right) - m_{fv}\omega_f^2\right]}{\mu\, k_v\left[\bar{k}_{sssi} - \omega_f^2 m_{fv} - k_v + (\kappa+\chi)\left(\bar{k}_{sssi} + \bar{k}_f\right)\right] + \kappa\bar{k}_f\left(m_{fv}\omega_f^2 - \bar{k}_{sssi} + k_v - \chi\left(\bar{k}_{sssi} + \bar{k}_f\right)\right)}. \tag{20}$$

Ultimately, optimal tuning parameters of the IViBa under harmonic excitation are obtained as

$$k_{IViBa} = \Re\left\{\bar{k}_{IViBa}\right\} \text{ and } c_{IViBa} = \frac{\Im\left\{\bar{k}_{IViBa}\right\}}{\omega_f} \tag{21}$$

where $\Re\{\bar{k}_{IViBa}\}$ and $\Im\{\bar{k}_{IViBa}\}$ are the real and imaginary parts of $\bar{k}_{IViBa}$ in Eq. (20), respectively.

Notably, for perfectly rigid ground connection of the inerter, i.e. for $\kappa \to \infty$ in Eq. (18), Eq. (20) simplifies as

$$\bar{k}_{IViBa} = \frac{k_v(\mu+1)[\bar{k}_{sssi}+\chi(\bar{k}_f+\bar{k}_{sssi})-m_{fv}\omega_f^2]}{\chi(\bar{k}_{sssi}+\bar{k}_f)+\bar{k}_{sssi}-\omega_f^2 m_{fv}-k_v(\mu+1)-\mu(\bar{k}_{sssi}/\bar{k}_f)k_v}. \quad (22)$$

If, additionally, $\mu = 0$, i.e. inertance $b = 0$, Eqs. (20) and (22) degenerate to the expressions for optimal ViBa design reported in [12]. Lastly, for $\kappa = 0$, the same expression for optimal ViBa design of Cacciola and Tombari [12] is again retrieved regardless of the value of the inertance b or, equivalently, of ratio μ. Note, however, that the latter case bears little practical significance corresponding to an inerter with a "free" second terminal.

3.3 Optimal H_2 IViBa tuning for broad-band (white noise) excitation

In case of white noise stationary random excitation $U_g(\omega)$ with constant-valued spectrum, minimization of peak u_{str} can be achieved by minimizing the second, *L_2*, norm of $H_{str}(\omega)$ leading to a H_2 optimal control design (e.g. [33,34]). That is,

$$\min_{\boldsymbol{\alpha}}\left\{\|H_{str}(\omega)\|^2 = \int_0^{\omega_{cut}} H_{str}^*(\omega)\, H_{str}(\omega) d\omega\right\} \text{ where } \boldsymbol{\alpha} = \{k_{IViBa}, c_{IViBa}\} \in \mathbb{R}_0^+ \quad (23)$$

in which $H_{str}^*(\omega)$ is the conjugate of $H_{str}(\omega)$ and ω_{cut} is a frequency value above which the integrand takes on negligible values. The above optimal tuning of the IViBa ensures that the displacement response variance of the structure is minimized under white noise excitation and, therefore, so does the peak u_{str} response [35]. In the ensuing numerical work, the default pattern search algorithm of MATLAB® is used to solve the minimization problem in Eq. (23) numerically.

4. NUMERICAL RESULTS

This section furnishes and discusses numerical results quantifying the effectiveness of H_∞ and H_2 optimally tuned IViBa with different inertial (i.e., mass and inertance) properties to reduce seismic displacement demands of the SDOF structural system in Figure 2. The presentation begins by describing an adopted benchmark mechanical model whose properties derive from a small-scale prototype specimen of a ViBa coupled with a SDOF oscillator.

4.1 Adopted benchmark model of a small-scale prototype specimen

Putting aside the IViBa properties k_{IViBa}, m_{IViBa}, c_{IViBa}, and b, the same, listed in Table 1, values of the remaining properties of the mechanical model in Figure 2 are assumed in all following numerical work. These values pertain to a physical small-scale ViBa prototype specimen used to control the response of a SDOF structure presented in detail in [12]. Specifically, all mass and stiffness properties are extracted directly from the manufactured prototype. Viscous damping coefficients are computed from the corresponding non-dimensional loss factor, η, using the expression

$$c = \frac{\eta k}{\omega_0}, \quad (24)$$

where $\omega_0 = 22.62$ rad/s is the fundamental natural frequency of the SDOF prototype oscillator accounting for soil compliance at its foundation. Note that Eq. (24) is strictly valid for harmonic input only and maps a hysteretic type of damping, widely used in SSI studies, according to which complex impedance is defined as $k(1 + i\eta)$, to viscous type of damping in which complex impedance is defined as $k + i\omega_0 c$ [32].

Table 1. Adopted mechanical properties for the model in Figure 2 corresponding to the small-scale prototype ViBa specimen in [12].

Property	**SDOF structure**	**SSI (structure)**	**SSI (IViBa)**	**SSSI**	**Inerter**
mass (kg)	$m= 0.590$	$m_f= 0.353$	$m_{f,IViBa}= 0.491$	-	$m_{f,I}= 0$
stiffness (N/m)	$k= 909.85$	$k_f= 640$	$k_{f,IViBa}= 760$	$k_{SSSI}= 315$	$k_{f,I}= 760$
loss factor	$\eta= 0.1$	$\eta_f= 0.1$	$\eta_{f,IViBa}= 0.1$	$\eta_{SSSI}= 0.02$	$\eta_{f,I}= 0.1$
damping coefficient (Ns/m)	$c= 4.0$	$c_f= 2.81$	$c_{f,IViBa}= 3.34$	$c_{SSSI}= 0.28$	$c_{f,I}= 3.34$

4.2 H_∞ IViBa tuning and assessment for harmonic base excitation

The problem of minimizing the peak steady state response of the SDOF structure in Figure 2 for the properties of Table 1 is herein considered for harmonic ground excitation (i.e., $U_g(\omega_f) = 1$) with frequency equal to the natural frequency of the SDOF structure with flexible basis (i.e., $\omega_f = \omega_0 = 22.62$ rad/s). To this aim, the optimization problem in Eq. (15) is solved to determine optimal positive IViBa stiffness, k_{IViBa}, and damping coefficient, c_{IViBa} for different values of IViBa mass, m_{IViBa}, and inertance, b. This is achieved by using the closed-form expressions in Eqs. (20) to (22). The performance of different optimal IViBa designs is assessed by examining frequency response functions (FRFs) of practical interest, computed by the magnitude of transfer functions in Eq.(14).

Whilst FRFs track performance in a wide frequency range, attention is herein focused mostly on vibration suppression at the natural structural frequency ω_0 which the considered H_∞ style IViBa tuning targets aiming for structure-oriented vibration control. Firstly, vibration suppression performance is compared for two optimal IViBa designs with total IViBa inertia (mass plus inertance) equal to the mass of the SDOF structure to be protected, i.e., $m_{IViBa} + b = m$. One design has a relatively large IViBa mass equal to 75% of the structural mass m and small inertance equal to 25% of structural mass, while the other design has relatively small IViBa mass and large inertance equal to 25% and 75% of the structural mass, respectively. Figures 3(a) and 3(b) plot the FRFs of the total SDOF structural displacement and of the relative structural displacement with respect to its foundation (i.e., deflection), respectively, for the two considered optimal IViBa designs. FRFs corresponding to the uncontrolled (no IViBa) structure as well as to a structure protected by an optimally designed ViBa ($b = 0$) with mass equal to the structural mass, $m_{IViBa} = m$, are superimposed on the same figures to facilitate comparisons. It is seen that the IViBa designs falls slightly short of the (much heavier) conventional ViBa in terms of structural response reduction at $\omega_f = \omega_0$ frequency. Specifically, the ViBa reduces steady-state structural response at resonance frequency by 97% compared to the uncontrolled structure, while a reduction of 96% and 94% is achieved for the IViBa with inertance $b = 0.25m$ and $b = 0.75m$, respectively. Therefore, for fixed total IViBa inertia, $m_{IViBa} + b$, structural performance at resonance frequency deteriorates marginally for lighter IViBas with larger inertance. This is a practically important result suggesting that the incorporation of the grounded inerter to the ViBa reduces the required ViBa mass with negligible compromise to structural performance at resonance assuming harmonic excitation. Furthermore, it is seen in Figure 3(c), which plots the FRF of the IViBa total displacement, that the motion amplitude of the internal IViBa unit with larger inertance and fixed total inertia is significantly smaller at the targeted resonance frequency.

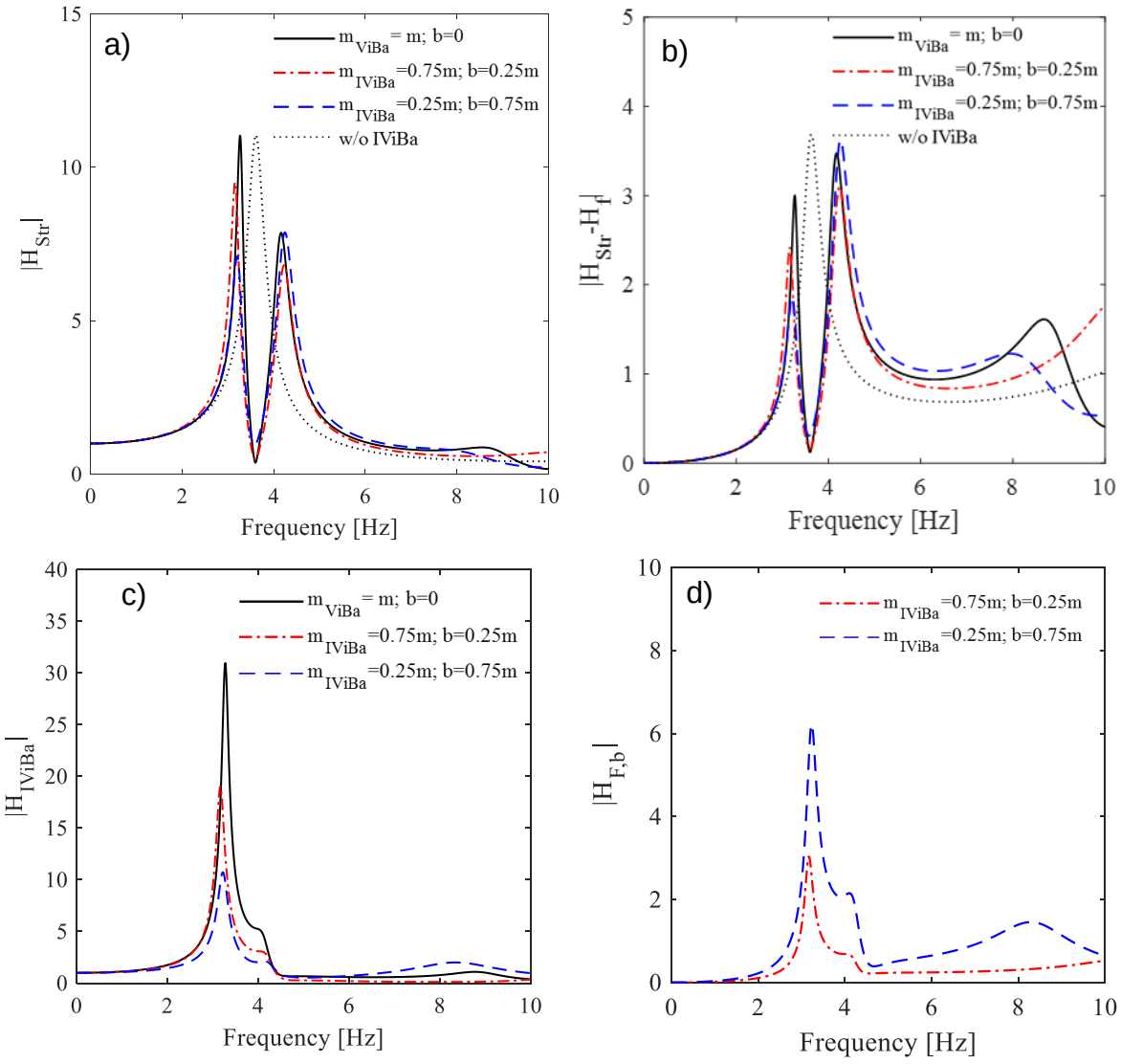

Figure 3 Frequency response functions of H_∞ optimally designed IViBa for various mass and inertance values of a) absolute structural displacement, b) relative structural displacement, c) IViBa mass displacement, and d) Inerter force

This is also a practically important result suggesting that the grounded inerter reduces demands for clearance in the IViBa unit which, ultimately, leads to more compact IViBas with reduced excavation cost and underground space usage. Nevertheless, it is seen in Figure 3(d), which plots the FRF of the inerter force, $H_{F,b} = b\omega^2|H_{IViBa} - H_{f,I}|$, that the benefits of reduced IViBa weight and volume with increasing inertance come at the cost of increased inerter forces that need to be transmitted to the ground. In this respect, the detailing of the inerter to the ground connection becomes critical. Moreover, looking away from the resonant frequency $\omega_f = \omega_0$ targeted but the considered H_∞ it is found that the increase of IViBa inertance for fixed total IViBa inertia has mixed effects to structural performance. IViBas with larger inertance reduce significantly the peak $|H_{str}(\omega)|$ value in Figure 3(a) but, at the same time, increase the peak structural deflection FRF, $|H_{str}(\omega) - H_f(\omega)|$. Therefore, increasing the inertance in H_∞ optimal IViBa at $\omega_f = \omega_0$ may have detrimental effect to structural performance for ground excitations with rich frequency content in the region of $\omega > \omega_0$.

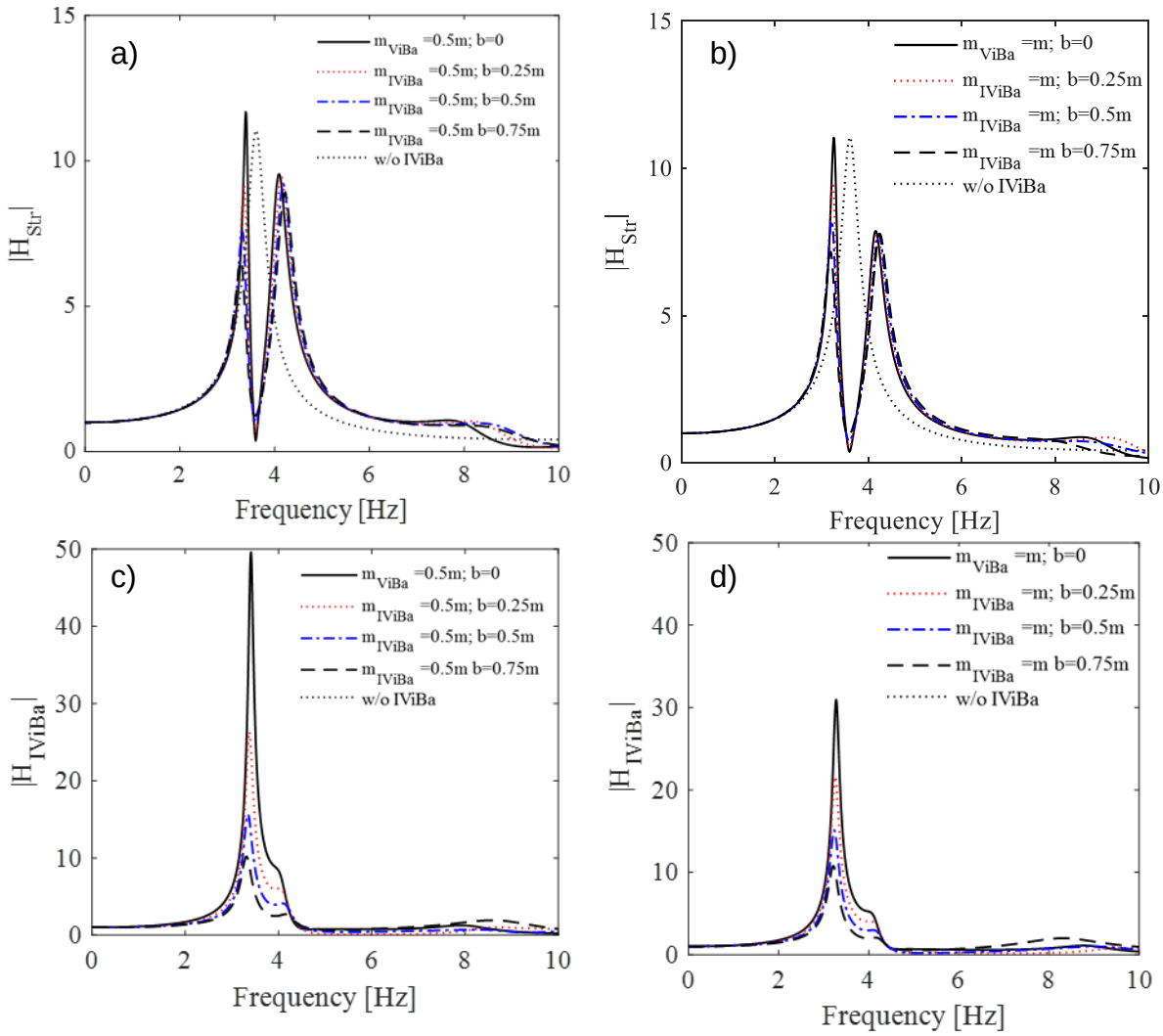

Figure 4. Frequency response functions of H_∞ optimally designed IViBa for fixed mass and for various values of inertance of a), b) absolute structural displacement for m_{IViBa}=0.5m, and m_{IViBa}=m, respectively, and c), d) IViBa mass displacement, for m_{IViBa}=0.5m, and m_{IViBa}=m, respectively.

Next, the influence of increasing inertance for fixed IViBa mass on the response of the SDOF structure and of the IViBa unit is examined by considering two different sets of optimally designed (I)ViBas with various inertance values: one set with fixed IViBa mass $m_{IViBa} = 0.5m$ and the other set with double the IViBa mass, $m_{IViBa} = m$. Figures 4(a) and 4(b) plot total displacement FRFs, $|H_{str}(\omega)|$, for $m_{IViBa} = 0.5m$ and $m_{IViBa} = m$ IViBa sets, respectively; the FRF of the uncontrolled structure is also superposed. It is seen that the IViBa suppresses effectively the $|H_{str}(\omega_o)|$ ordinate by over 92% for all inertance values considered and for both m_{IViBa} values.

It is further seen that the increase of inertance reduces significantly the peak value of the leftmost $|H_{str}(\omega)|$ lobe while it moves its location to lower frequencies (i.e., away from the resonant frequency). However, the peak value of the second $|H_{str}(\omega)|$ lobe is mostly leveraged through the m_{IViBa} property. Lastly, Figures 4(c) and 4(d) plot IViBa mass displacement FRFs, $|H_{IViBa}(\omega)|$, for the same sets of (I)ViBas considered previously. It is confirmed that the peak response displacement of the IViBa internal unit decreases significantly for increasing values of inertance.

4.3 Optimal H_2 IViBa tuning for broad-band excitation

This sub-section presents FRF data for IViBa optimally designed to minimize the root-mean-square (RMS) displacement response of the SDOF structure in Figure 2 subject to broad-band (i.e., clipped white noise) stochastic excitation given as $U_g(\omega) = 1$ for $0 \leq \omega \leq \omega_{cut} = 62.84$ rad/s = 10 Hz. This style of optimal design is mostly excitation-related (rather than structure-dependent) recognising that earthquake induced ground motions are broadband in nature. System properties of Table 1 are adopted as before and the optimization problem in Eq. (23) is solved numerically to determine optimal IViBa stiffness, k_{IViBa}, and damping coefficient, c_{IViBa}, values for different values of IViBa mass, m_{IViBa}, and inertance, b. Figure 5 furnishes FRF plots for (I)ViBas with the same inertial properties previously considered in Figure 3 but now optimally designed in the H_2 sense minimizing the area below the $|H_{str}(\omega)|$ FRF. Optimal (I)ViBa design parameters obtained from numerical optimization are reported in Table 2. It is deduced from Figures 5(a) and 5(b) that replacement of part of the ViBa mass with inertance such that the total inertia remains the same, $m_{IViBa} + b = m$, results in more effective vibration suppression across a wide range of frequencies. However, an increase of the inertance contribution from 25% to 75% of the total inertia reduces the vibration suppression performance. This finding suggests that higher inertance contribution to the total inertia may not result in improved vibration suppression for ground motion with relatively high frequency content. At the same time, motion amplitude of the IViBa mass unit reduces significantly in the frequency range around the SDOF structure natural frequency, ω_0, but increases at higher frequencies for the case of $b = 0.75m$ as seen in Figure 5(c). In fact, in the latter case, the $|H_{IViBa}(\omega)|$ FRF becomes bi-modal with a second local maximum attained at a frequency related to resonance of the internal IViBa unit with respect to the grounded inerter element. Indeed, the second lobe of the $|H_{IViBa}(\omega)|$ FRF is located at about $\sqrt{k_{IViBa}/b}$ rad/s frequency. This second/higher resonant frequency introduced to the IViBa unit by the grounded inerter with $b = 0.75m$ is even more apparent in the inertance force FRF plots of Figure 5(d).

Table 2 Optimal IViBa design parameters for the IViBas considered in Figure 6.

IViBa inertial properties	$m_{IViBa} = m$ $b = 0$	$m_{IViBa} = 0.75m$ $b = 0.25m$	$m_{IViBa} = 0.25m$ $b = 0.75m$
k_{IViBa} [N/m]	439.9	985.5	1421.6
c_{IViBa} [Ns/m]	4.41	20.31	76.58

Table 3 Optimal values of the IViBa used for the cases in Figure 7 for $m_{IViBa} = 0.5m$.

IViBa inertance	$b = 0$	$b = 0.25m$	$b = 0.5m$	$b = 0.75m$
k_{IViBa} [N/m]	195.52	360.61	667.38	1269.00
c_{IViBa} [Ns/m]	1.18	3.09	9.14	39.65

Table 4 Optimal values of the IViBa used for the cases in Figure 7 for $m_{IViBa} = m$.

IViBa inertance	$b = 0$	$b = 0.25m$	$b = 0.5m$	$b = 0.75m$
k_{IViBa} [N/m]	439.85	663.09	1048.20	1416.40
c_{IViBa} [Ns/m]	4.41	9.02	23.38	82.05

More importantly, Figure 5(d) shows an increase of inerter force with increasing inertance across all frequencies suggesting that for broadband excitation larger inertance force does not necessarily lead to improved motion suppression either for the structure or for the IViBa unit.

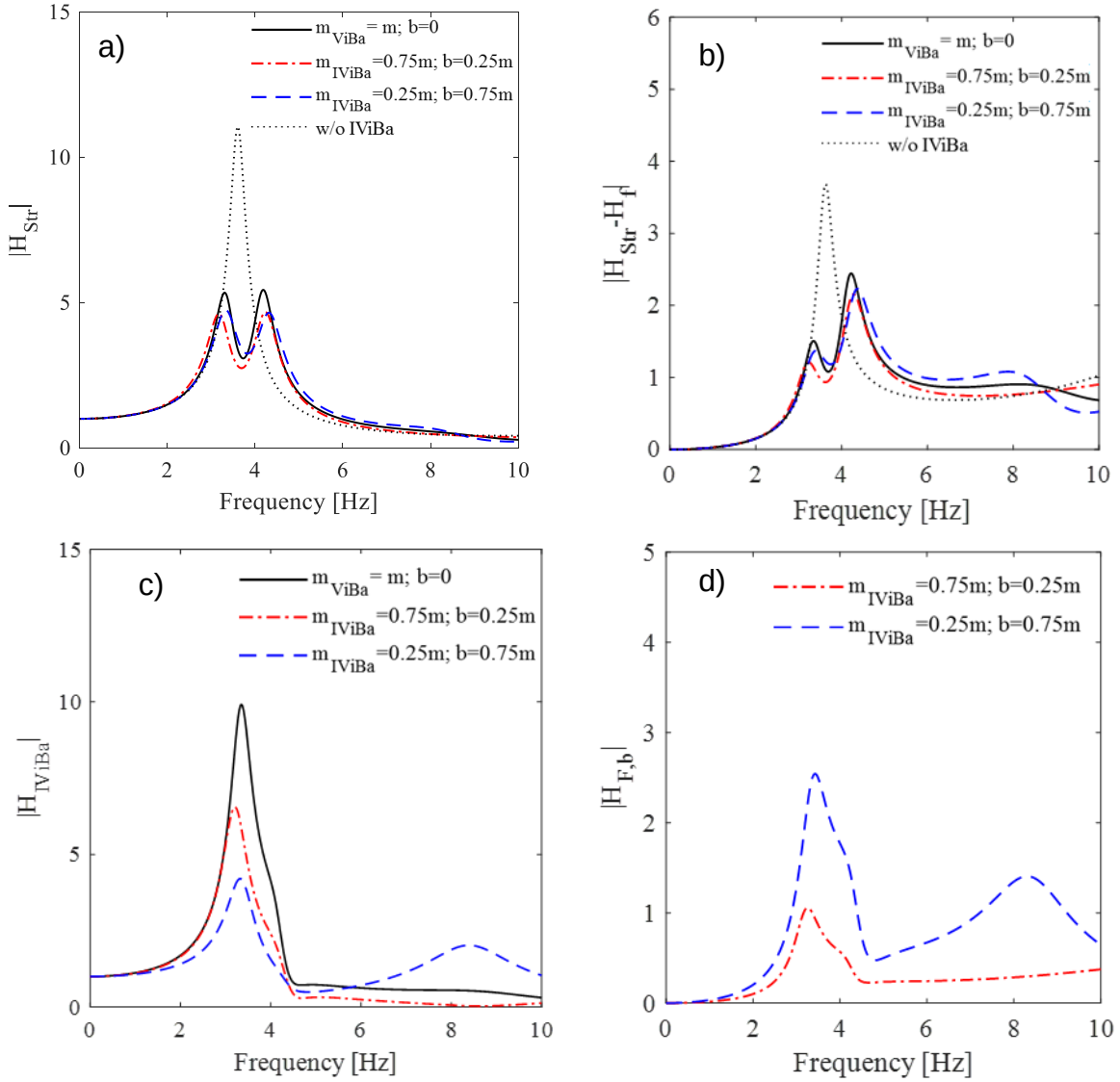

Figure 5. Frequency response functions of H_2 optimally designed IViBa for various mass and inertance values of a) absolute structural displacement, b) relative structural displacement, c) IViBa mass displacement, and d) Inerter force

Attention is next turned to quantifying the effect of increasing inertance for fixed IViBa mass in H_2 optimally designed IViBas. Figures 6(a) and 6(b) plot $H_{str}(\omega)$ FRFs for fixed IViBa mass equal to $m_{IViBa} = 0.5m$ and to $m_{IViBa} = m$, respectively, and for several inertance values. The related H_2 optimal (I)ViBa parameters are reported in Tables 3 and 4 for the two different IViBa mass values. It is evidenced that the area below the FRF curves reduces with increasing inertance. For the relatively light IViBa (Figure 6a), larger reductions are observed around the second (rightmost) FRF lobe. For the heavier IViBa (Figure 6b) the increase of inertance above m is locally detrimental around the second lobe, though still beneficial across the whole range of excitation frequencies. Further, Figures 6(c) and 6(d) plot $H_{IViBa}(\omega)$ FRFs for the above H_2 optimally designed IViBas. It is seen that the increase of inertance suppresses significantly the IViBa unit motion at frequencies close to the structural natural frequency ω_0.

However, as the inertance increases a second lobe appears within the frequency range of interest [0 10] Hz with increasing amplitude centred at about $\sqrt{k_{IViBa}/b}$ rad/s rendering the $|H_{IViBa}(\omega)|$ FRF bi-modal.

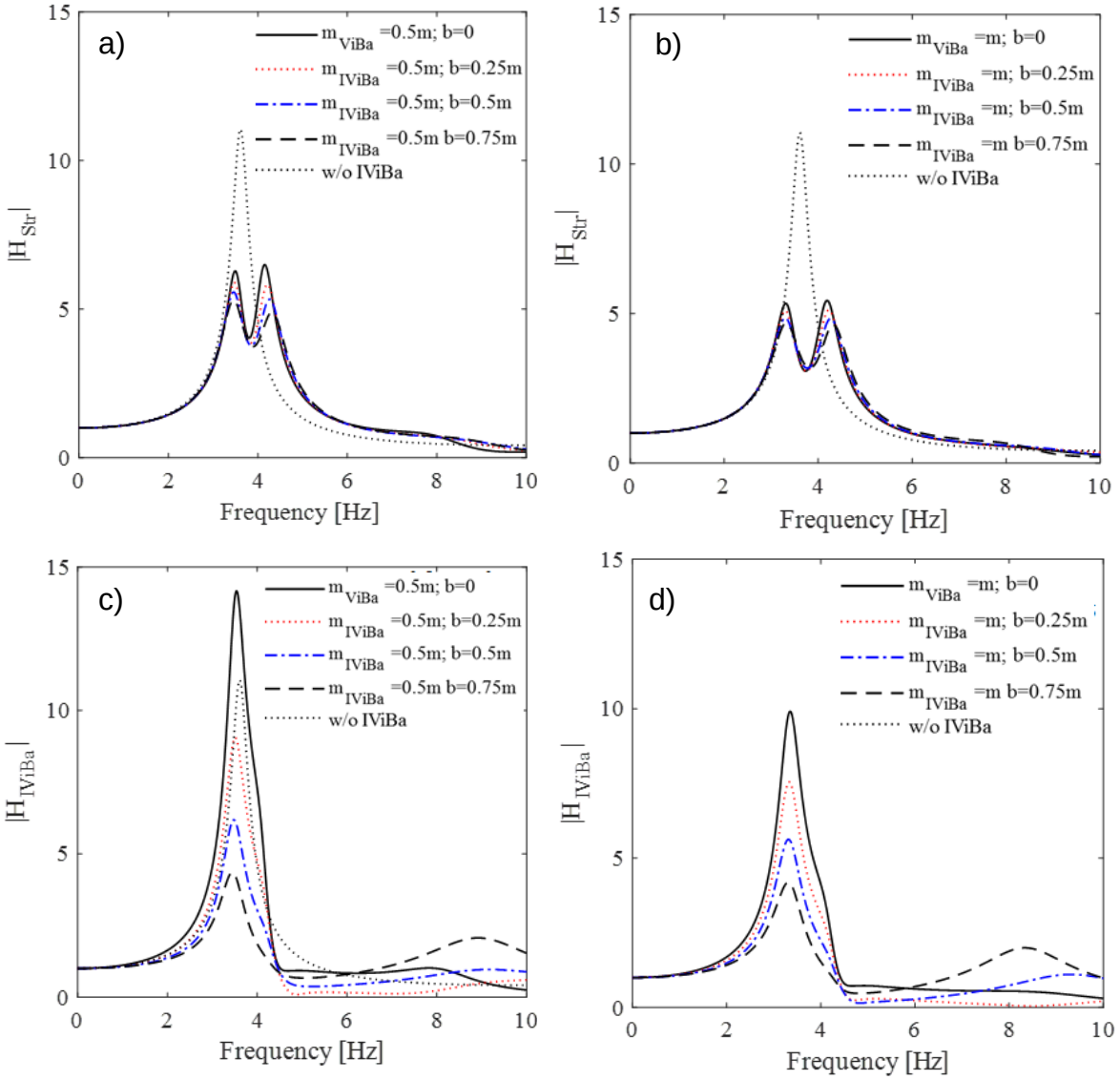

Figure 6 Frequency response functions of H_2 optimally designed IViBa for fixed mass and for various values of inertance of a), b) absolute structural displacement for m_{IViBa}=0.5m, and m_{IViBa}=m, respectively, and c), d) IViBa mass displacement, for m_{IViBa}=0.5m, and m_{IViBa}=m, respectively.

4.4 Assessment of H_∞ and H_2 optimal IViBa design to broadband excitation

The two different IViBa design approaches discussed above are remarkably different as one, the H_∞, aims to structure-dependent tuning of the IViBa to the frequency that mostly excites the structure to be protected while the other, the H_2, tunes the IViBa to achieve more balanced vibration suppression of the structure across a wide range of frequencies. To facilitate a comparison, Figure 7(a) plots vis-à-vis $|H_{str}(\omega)|$ curves obtained by IViBa optimally designed in the H_∞ (tuned for harmonic excitation at the structural frequency ω_0) and H_2 (tuned for white noise excitation) sense with $m_{IViBa} = m$ and $b = 0.75$. It is seen that H_∞ optimal tuning achieves significant $|H_{str}(\omega)|$ ordinate reductions at ω_0 compared to H_2 optimal tuning, while the latter achieves flatter $|H_{str}(\omega)|$ ordinates on a wide frequency range.

Further, Figure 7(b) plots the same data for the case of ViBa with $m_{IViBa} = m$. It is seen that whilst ViBa is slightly more effective to control resonant harmonic excitation, the IViBa achieves better overall suppression of the $|H_{str}(\omega)|$ ordinates at a wide range of frequencies for both H_∞ and H_2 tuning.

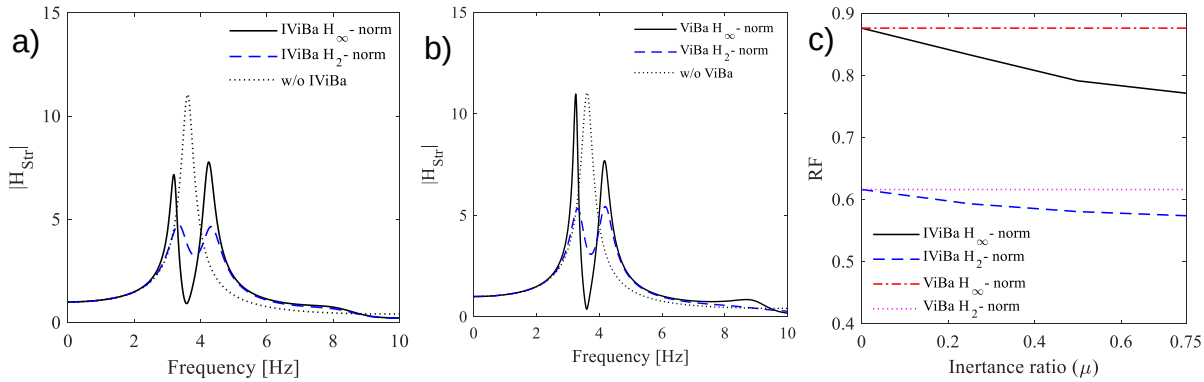

Figure 7 Comparison of H_∞ and H_2 tuning approaches to the $H_{str}(\omega)$ FRFs for a) IViBa with $m_{IViBa} = m$ and $b = 0.75m$, b) ViBa with $m_{IViBa} = m$ c) reduction factors.

Further to the above comparative assessment of H_∞ and H_2 (I)ViBa tuning approaches in terms of $|H_{str}(\omega)|$ FRF, the following reduction factor (RF) index

$$RF = \frac{\int_0^{\omega_{cut}} H_{str}^*(\omega) H_{str}(\omega) d\omega}{\int_0^{\omega_{cut}} H_{str,unc}^*(\omega) H_{str,unc}(\omega) d\omega} \tag{25}$$

is herein used to quantify structural response reduction to broadband excitation. In the last equation, $H_{str,unc}$ is the transfer function of the uncontrolled SDOF structure and ω_{cut} is taken equal to 10Hz. Figure 7(c) plots the RF as a function of the inertance for (I)ViBa optimally designed in the H_∞ and H_2 sense for $m_{IViBa} = m$. Expectedly, H_2 optimization yields smaller RF values since it involves the minimization of an objective function which is similar to the definition of the RF in Eq. (25). It is further seen that performance improvement saturates as the inertance increases for both optimal design approaches. This trend is in alignment with trends observed in optimal designed TMDs coupled with a grounded inerter for white noise excitation [23] and for harmonic excitation [24]. Lastly, it is noted that the IViBa with increasing inertance does not offer significant RF improvement compared to the ViBa. However, the practically most important advantage of the IViBa compared to ViBa is mass reduction for fixed target performance which is quantified, discussed, and assessed in the following sections.

4.5 Mass reduction and soil compliance effects quantification

In previous sections, attention was primarily focused on quantifying and discussing IViBa performance assessment for varying (increasing) inertance. Nevertheless, the main motivation of coupling the ViBa with a grounded inerter is to reduce the required weight/volume of the ViBa unit as discussed in the introduction. To quantify mass reduction achieved by the grounded inerter, Figure 8(a) plots the RF in Eq.(25) for H_2 optimally tuned IViBa with various fixed inertance values as function of m_{IViBa} measured as percentage reduction the reference value $m_{IViBa} = m$, (i.e. IViBa mass equal to the mass of the SDOF structure). As expected, all RF curves increase monotonically with reducing IViBa mass confirming that better vibration suppression is achieved by increasing the (I)ViBa mass. However, it is mostly important to note in this plot that the RF curves shift to the right (i.e., towards larger IViBa mass reductions) as inertance increases. This means that as inertance increases the same structural performance is achieved for reduced IViBa mass. To illustrate

quantitatively this point, Figure 8(a) indicates the RF=0.62 value achieved by the H_2 optimally tuned ViBa with $m_{ViBa} = m$ (i.e., reference mass value used in scaling the x-axis of the graph) and reports mass reduction values at which the RF curves for IViBas with different inertance intersect with the RF=0.62 barrier. It is seen that significant mass/weight reduction for fixed (targeted) performance RF=0.62 is achieved by the inclusion of a grounded inerter with increasing inertance. Specifically, IViBas with inertance equal to 25%, 50%, and 75% of the IViBa mass achieve the same structural response reduction performance with the ViBa having mass equal to the structure mass but with reduced mass/weight of 11%, 19%, and 27%, respectively.

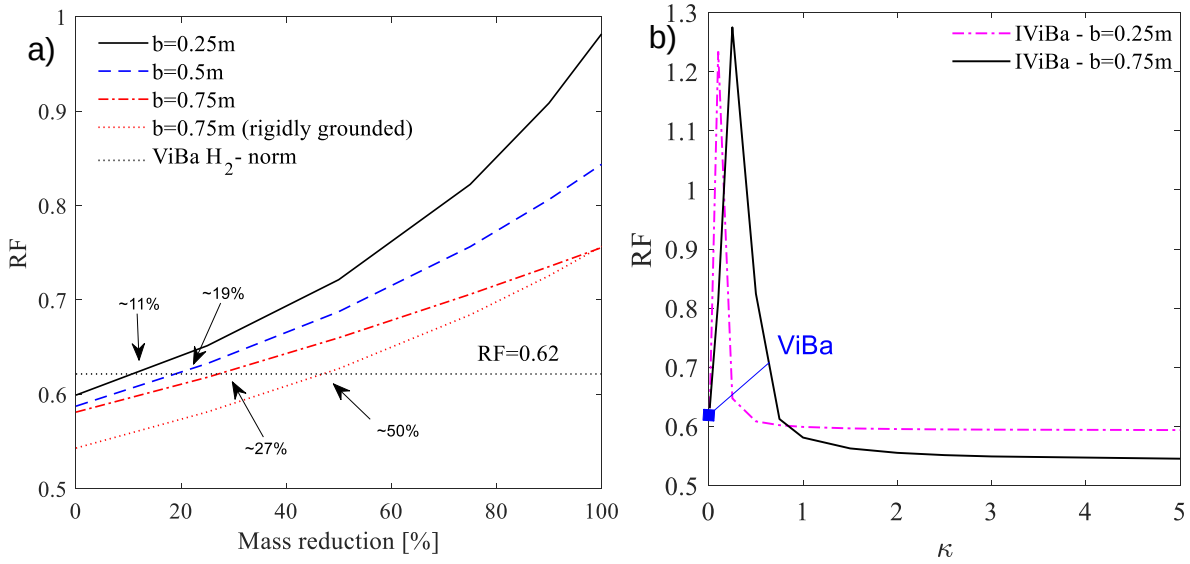

Figure 8. Reduction factor in Equation (16) for various $\boldsymbol{H_2}$ optimal IViBa as function of a) IViBa mass reduction from $\mathbf{m_{IViBa}} = \mathbf{m}$, b) magnitude of inerter-to-ground rigidity connection factor $\boldsymbol{\kappa}$ in Eq. (10).

Interestingly, the above significant mass/weight reductions for fixed performance enabled by the grounded inerter become more considerable with stiffer inertance-soil connection. To highlight this point, note that in all thus far considered cases the inertance-to-soil connection had the same rigidity ratio in Eq.(10) $\kappa = (k_{f,IViBa} + i\omega_f c_{f,IViBa})/(k_{f,I} + i\omega_f c_{f,I}) \cong |\kappa| = 1.1875$ (see Table 3). This is based on the assumption that the soil stiffness used in capturing SSI for the IViBa containment is the same for SSI associated with the inerter connection to the ground (i.e., $k_{f,IViBa} = k_{f,I}$ as well as $c_{f,IViBa} = c_{f,I}$ in Table 3). Plotted in Figure 9(a) is an RF curve for inertance 75% the IViBa mass and an inerter rigidly connected to the ground (i.e., $|\kappa|$=5). It is observed that the latter IViBa with inerter rigidly connected to the ground requires only half the mass (i.e., mass reduction of about 50%) of the reference ViBa to achieve the same performance, RF=0.62, as the reference ViBa. This is almost half mass less compared to the IViBa with same inertance but non-rigid inerter-to-ground connection, i.e. $|\kappa|$=1.1875. The above results demonstrate that the mass reduction effect of the grounded inerter to the (I)ViBa depends significantly on the soil compliance which, unless special soil fortification measures are taken, is site-specific and depends on the soil properties. To this end, Figure 8(b) plots the RF in Eq.(25) for H_2 optimally tuned IViBa with $b = 0.75m$ as a function of the magnitude of the rigidity factor κ to parametrically investigate the effect of soil compliance at the inerter-to-ground connection on the effectiveness of IViBa for structural vibration suppression. IViBa vibrations suppression effectiveness is maximised for perfectly rigid connection (i.e. $\kappa \to \infty$) . It is seen that for low values of $\kappa < 0.85$ reflecting

soft soil conditions and/or poor/compliant inerter-to-ground connection, the ViBa with same mass (corresponding to $\kappa = 0$ as discussed in section 3.2) is actually performing better than the IViBa. This is a practically most important result suggesting that special care is necessitated to ensure sufficient rigidity at the inerter to the ground connection. If sufficient rigidity is not guaranteed (e.g., due to soft soil conditions in conjunction with large inerter forces) then the remedy is to reduce inertance b. To illustrate the latter point, Figure 8(b) superposes the RF for H_2 optimally tuned IViBa with $\mathrm{b} = 0.25m$. Whilst the latter IViBa with relatively low inertance performs worse than the former with $\mathrm{b} = 0.75m$ for $\kappa > 1$, it achieves lower RF than the ViBa for inerter-to-ground rigidity connection as low as $\kappa = 0.4$ while it significantly outperforms the large inertance IViBa with $\mathrm{b} = 0.75m$ for $0.3 < \kappa < 0.90$. It is to be noted, of course, that consideration of lower inertance IViBa limits the beneficial weight reduction effect for fixed performance of the grounded inerter (see Figure 8a). The latter consideration entails that (soft) soil conditions will govern the selection of IViBa inertial properties (i.e., mass and inertance) in practical applications. Further investigation of this aspect of IViBa design falls beyond the scope of this study and is left for future work.

4.6 Time-domain performance of H_2 optimal IViBa for non-stationary colored base excitation

The previously quantified IViBa mass reduction/replacement effect of the grounded inerter assumed ideal stationary band-limited white noise excitation. Nevertheless, recorded seismic ground motions have non-white frequency content, which is primarily dominated by local soil deposits properties, while they are characterised by non-stationary in time amplitude. Hence, it is deemed essential to herein verify the achieved performance of the H_2 optimally tuned IViBas discussed in Figure 9(a) under colored and time-evolving amplitude seismic excitation. To this aim, a suite of 100 artificial non-stationary in amplitude ground acceleration time-histories are generated and the response of the mechanical system in Figure 2 is obtained by solving the governing equations of Eq.(2) via standard time-domain integration in a Monte Carlo simulation (MCS) based context. The 100 time-histories are time-enveloped/modulated realizations of a zero-mean stationary Gaussian stochastic process defined in the frequency domain by a one-sided power spectral density (PSD) function given as [36]

$$\mathrm{G}(\omega) = \frac{\omega_\mathrm{g}^4 + 4\zeta_\mathrm{g}^2\omega^2\omega_\mathrm{g}^2}{\left(\omega_\mathrm{g}^2 - \omega^2\right)^2 + 4\zeta_\mathrm{g}^2\omega^2\omega_\mathrm{g}^2} \cdot \frac{\omega^4}{\left(\omega_\mathrm{f}^2 - \omega^2\right)^2 + 4\zeta_\mathrm{f}^2\omega^2\omega_\mathrm{f}^2}. \tag{26}$$

In the above equation, the constant parameters take on the values $\omega_g = 7.49$ rad/s, $\omega_f = 2.14$ rad/s, $\zeta_g = 0.84$, and $\zeta_f = 1.15$ yielding a PSD function of a stationary stochastic process with frequency content compatible to the seismic response spectrum of the European seismic code, Eurocode 8 [37], for ground type C derived in [38]. The adopted (target) PSD function is plotted in Figure 9(a). On the same graph, the mean PSD estimate of 100 time-histories generated using the standard spectral representation simulation method [39] is superposed achieving satisfactory level of compatibility in the mean sense with the target PSD function. These time-histories are multiplied in time using the following modulating deterministic envelop function [40]

$$f(t) = \begin{cases} \left(\frac{t}{t_1}\right)^2 & t < t_1 \\ 1 & t_1 \le t \le t_2 \\ e^{-\beta(t-t_2)} & t > t_2 \end{cases} \tag{27}$$

in which $\beta = \frac{9}{T_s}$, $t_1 = \frac{1.5}{\beta}$, $t_2 = \frac{10.5}{\beta}$ (see e.g. [41]) and the length of the stationary part of the time history is set to $T_s = 15s$. An arbitrarily selected artificial ground motion acceleration

time-history (i.e., realization of the considered non-stationary stochastic process) out of the 100 generated is shown in Figure 9(b).

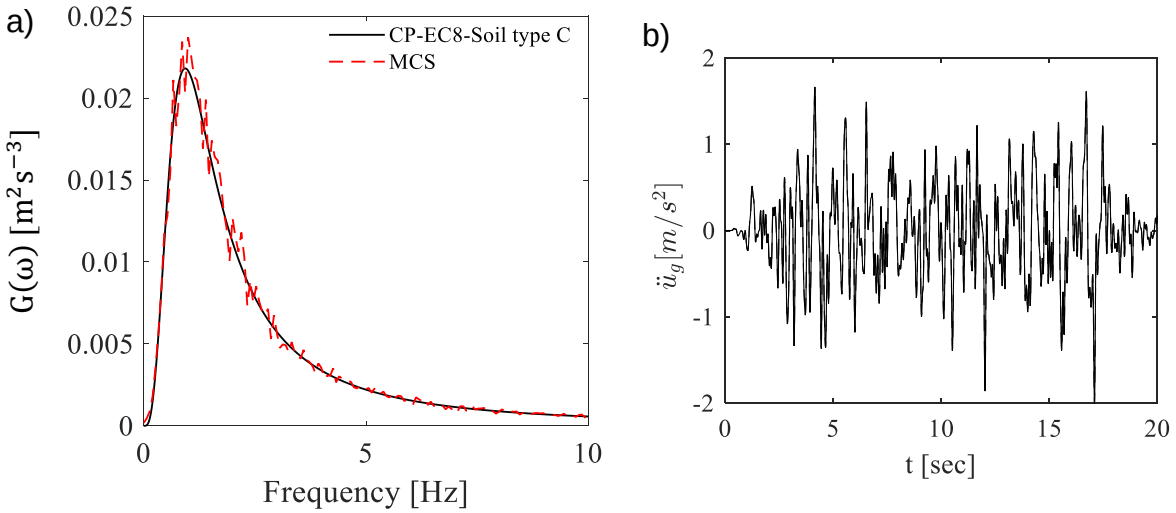

Figure 9 Quasi-stationary seismic excitation: a) Power spectral density function and b) arbitrary selected time-domain realization

Figure 10 reports selective response histories of the SDOF structure in Figure 2 for the considered quasi-stationary stochastic excitation for three H_2 optimally tuned IViBas with $b = 0.75m$ and different $\mathrm{m_{IViBa}}$ and for the unprotected structure (i.e., with no IViBa). Figure 10a plots mean PSD estimates of the structural acceleration averaged over the 100 structural response acceleration time-histories. Figure 10b shows arbitrarily selected structural response acceleration time-histories while in Figure 10c samples of relative response time-histories are reported. An estimate of the RF defined in Eq.(25) is further reported in Table 5 in which the integrals are computed from the mean value of the variances obtained through time-domain statistics for each structural response acceleration time-history.

Focusing first the attention on the left and the middle panel columns in Figure 10, it is noted that the two examined IViBas are those with $b = 0.75m$ and fixed RF=0.62 performance for white noise excitation indicated in Figure 8(a) for compliant and for perfectly rigid inerter-to-ground connection, respectively. Specifically, the IViBa with compliant connection has mass $\mathrm{m_{IViBa}} = 0.73\mathrm{m}$ while the IViBa with rigid connection has mass $\mathrm{m_{IViBa}} = 0.50\mathrm{m}$ which correspond to 27% and 50%, respectively, achieved mass reduction from the reference mass, $\mathrm{m_{IViBa}} = \mathrm{m}$, for white noise excitation assumed in Figure 8a. Importantly, it is seen that the RF estimates obtained from the MCS response data is almost the same with the fixed RF level in Figure 8a. This finding verifies that the two IViBas perform as expected under non-stationary coloured excitation which further confirms the mass/weight reduction gains achieved by the inerter with different levels of connection rigidity to the ground in a performance-based design setting.

Moreover, the ratios of mean peak structural response deflection (relative displacement), $\max_t |u_{str}(t) - u_f(t)|$, and acceleration, $\max_t |\ddot{u}_{str}(t)|$, of the controlled over the uncontrolled structure are also furnished in Table 5 as these quantities are of interest to practical seismic assessment of structures: the former relates well to structural damage while the latter relates well to damage in non-structural components/fittings and in sensitive equipment housed within buildings. It is noted that the reduction of the relative displacement is only used as part of the assessment and it is not directly related to the optimization procedure.

If so desired, H_2 optimization can be applied by using the relative displacements in the optimization procedure in which case Eq. (23) needs to be modified accordingly.

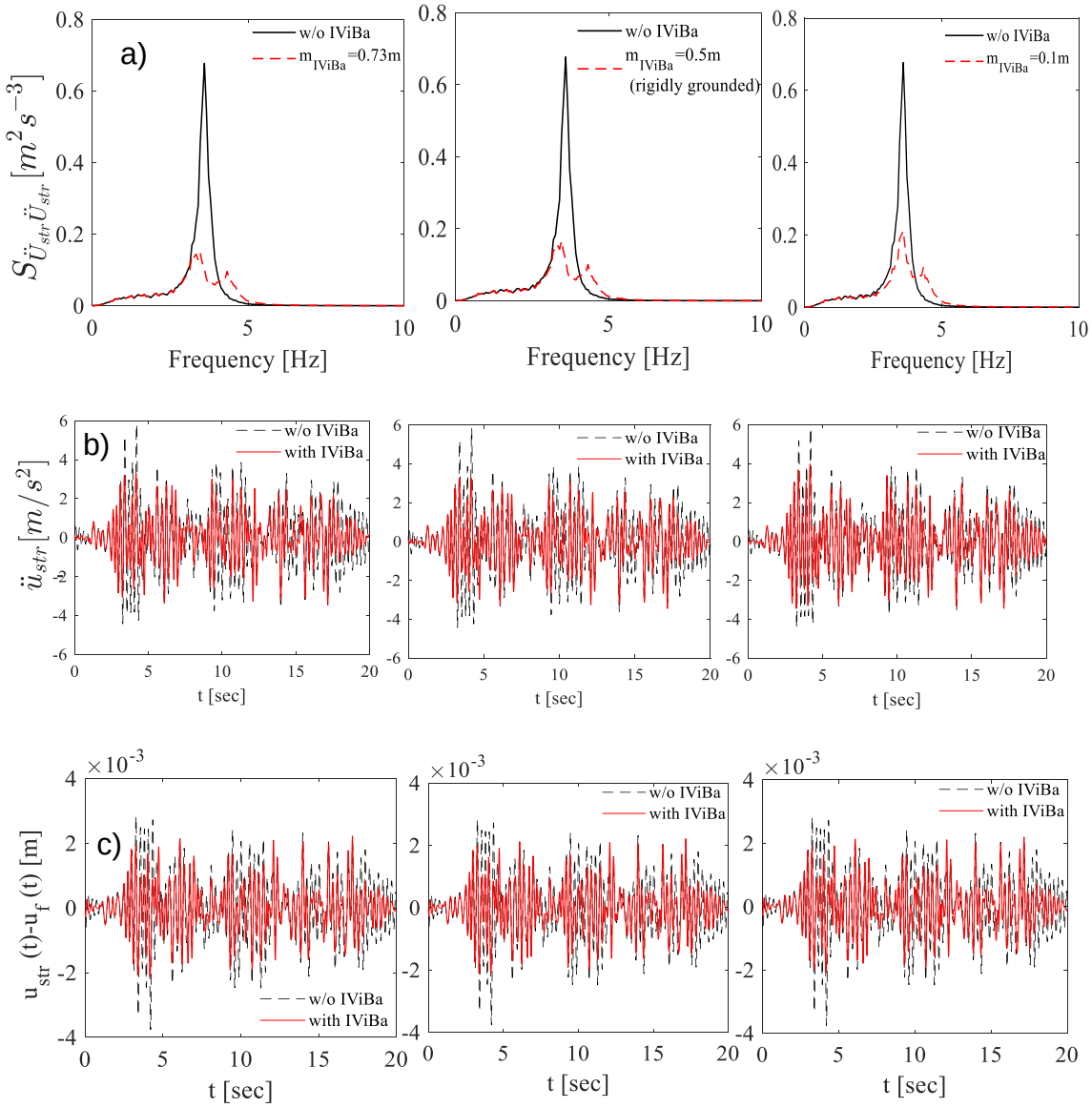

Figure 10 Response data comparison of the SDOF structure in Figure 2 to the quasi-stationary excitation of Figure 9 with and without IViBa protection for H_2 optimally tuned IViBas with b = 0.75m and three different m_{IViBa} values a) Response acceleration power spectral density functions; b) samples of response accelerations time-histories; c) samples of response accelerations relative displacements.

Table 5: Comparison between reduction factors (RFs) obtained through Eq (25) and through response history analyses.

Case	RF - H_2	RF - MCS	Relative error [%]	Peak reduction [%]	
				Abs acc.	Rel. displ.
$m_{IViBa} = 0.73m$	0.62	0.60	-3.60	21.01	21.06
$m_{IViBa} = 0.5m$ Rigidly grounded	0.62	0.60	-2.66	20.74	20.78
$m_{IViBa} = 0.1m$	0.73	0.67	-9.8	16.40	16.52

Lastly, an additional H_2 optimal IViBa case, not previously considered, is studied in the right panel column of Figure 11 with same inertance, $b = 0.75m$, and compliant inerter-to-ground connection and with mass $\mathrm{m_{IViBa}} = 0.1\mathrm{m}$ which is of the order considered in typical TMDs attached to the top floor of building structures for seismic performance improvement [4]. It is seen that this lightweight IViBa achieves an RF=0.7 for the considered Eurocode 8 response spectrum compatible non-stationary ground excitation while reduces peak deflection and acceleration compared to the unprotected structure by 16.4% and 16.52% respectively. In this regard, it is concluded that a grounded inerter with sufficient high inertance allows for compact and lightweight IViBas (i.e., with weight similar to the weight of TMDs attached to structures) capable for significant peak response reduction of seismically excited structures with no intrusive structural modification.

5. CONCLUDING REMARKS

The previously established by the first two authors ViBa has been herein extended by incorporating a grounded inerter acting as a mass/inertial amplifier to enhance the ViBa efficiency and applicability for non-invasive seismic protection of existing structures. In this setting, the potential of the resulting IViBa configuration embedded to the ground has been explored to suppress the motion of an adjacent seismically excited structure modelled as a SDOF linear oscillator by exploiting the SSSI mechanism. To this aim, a 5-DOF dynamical system has been established accounting for SSI effects due to soil compliance in the SDOF structure, the IViBa containment as well as in the inerter-to-the-ground connection and pertinent equations of motion and transfer functions reported. Two different types of optimal IViBa tuning have been pursued. The first is structure-dependent H_∞ design aiming to minimise the peak response of the SDOF structure at its resonance frequency for which closed-form optimal design parameters formulae were derived. The second is H_2 design aiming to minimize the RMS structure response displacement which was solved numerically.

Selective numerical results have been reported pertaining to a small-scale ViBa prototype specimen to explore the influence of the inertance property of the grounded inerter to the required IViBa mass for effective seismic response mitigation of a SDOF linear oscillator which was reported to be impractically large in many cases in previous work by the first two authors. It was herein found that trading inertance to mass in (I)ViBas with fixed total inertia (i.e., mass plus inertance) for reduced IViBa weight does not improve structural performance of the SDOF structure: peak displacement deteriorates especially in higher frequencies. Nevertheless, the increase of inertance for fixed IViBa mass is always beneficial for structural performance and for reducing required clearance within the IViBa unit enabling more compact IViBas and reduced excavation cost. These improvements, however, come at the expense of increased inertance forces that need to be accommodated by the inerter device and by the supporting ground.

Most importantly, it has been found that the grounded inerter does achieve significant mass/weight reduction for fixed targeted structural performance dependent on the combined effects of inertance and achieved level of rigidity at the connection: higher inertance in conjunction with sufficiently rigid inerter-to-ground connection yields higher weight gains (reductions). This has been verified for both stationary white noise as well as for colored non-stationary in amplitude stochastic excitations, the latter involving the consideration of a suite of 100 artificial non-stationary accelerograms compatible with the Eurocode 8 response spectrum for seismic structural design in a Monte Carlo simulation context. Interestingly, pertinent parametric analyses with regards to inerter-to-ground connection rigidity indicate that in less rigid and/or softer (i.e., more compliant) supporting soil conditions, the consideration

of large inertance may actually deteriorate structural performance compared to the ViBa. In such cases lowering the inertance is beneficial in relaxing the range of the level of connection rigidity required for the grounded inerter to contribute positively to the ViBa performance. This is readily attributed to the fact that lower inertance attracts smaller inerter forces alleviating the problem of high compliant inerter-to-ground connection. In this respect, careful design and assessment of inerter-to-ground connection rigidity is most critical in safeguarding and fully exploiting the beneficial effects of grounded inerter for mass/weight IViBa reduction. In practical applications, this may be readily leveraged by using several inerter devices arranged in parallel such that total required inerter force is distributed evenly in space reducing transmitted stress to the ground.

Overall, the herein reported numerical results demonstrate that the consideration of a grounded inerter facilitates significantly potential practical implementation of the ViBa for non-invasive seismic protection of single structures amenable to be modelled as SDOF systems as it lowers required IViBa weight leading to lower excavation and material and underground space usage costs. Still, further research is warranted to explore IViBa potential for practical implementation for seismically excited structures with significant higher modes contribution, as well as for clusters of structures in urban environments supported by pertinent numerical and experimental work. Ultimately, gauging IViBa effectiveness for seismic protection of real-life structures requires large-scale experimental validation involving field deployment. Further, full-scale field testing provides a straightforward way to quantify differences to the ground excitation experienced by the IViBa and neighbouring structures and their effect to IViBa optimal design. These considerations, left for future work, will inform IViBa optimal design maximizing its potential to become a competitive solution for the seismic protection of existing structures.

REFERENCES

[1]I. Avramidis, A. Athanatopoulou, K. Morfidis, A. Sextos, and A. Giaralis, Eurocode-Compliant Seismic Analysis and Design of R/C Buildings Concepts, Commentary and Worked Examples with Flowcharts. Cham: Springer International Publishing ;, 2016.

[2]T. T. Soong and G. F. Dargush, Passive energy dissipation systems in structural engineering. Chichester ; New York: Wiley, 1997.

[3]M. De Angelis, S. Perno, and A. Reggio, “Dynamic response and optimal design of structures with large mass ratio TMD,” Earthquake Engineering & Structural Dynamics, vol. 41, no. 1, pp. 41–60, Jan. 2012.

[4]E. Matta, “Lifecycle cost optimization of tuned mass dampers for the seismic improvement of inelastic structures,” Earthquake Engineering & Structural Dynamics, vol. 47, no. 3, pp. 714–737, Mar. 2018.

[5]F. Naeim and J. M. Kelly, Design of seismic isolated structures: from theory to practice. New York: John Wiley, 1999.

[6]M. N. Fardis, Seismic design, assessment and retrofitting of concrete buildings: based on EN-Eurocode 8. Dordrecht ; New York: Springer, 2009.

[7]A. J. Kappos and E. G. Dimitrakopoulos, “Feasibility of pre-earthquake strengthening of buildings based on cost-benefit and life-cycle cost analysis, with the aid of fragility curves,” Natural Hazards, vol. 45, no. 1, pp. 33–54, Apr. 2008.

[8]R. D. Woods, “Screening of surface waves in soils,” J. Soil Mech. Found. Eng. Div., vol. 94, no. 4, pp. 951–979, 1968.

[9]S. Krödel, N. Thomé, and C. Daraio, "Wide band-gap seismic metastructures," Extreme Mechanics Letters, vol. 4, pp. 111–117, Sep. 2015.

[10]V. K. Dertimanis, I. A. Antoniadis, and E. N. Chatzi, "Feasibility Analysis on the Attenuation of Strong Ground Motions Using Finite Periodic Lattices of Mass-in-Mass Barriers," Journal of Engineering Mechanics, vol. 142, no. 9, p. 04016060, Sep. 2016.

[11]A. Palermo, S. Krödel, A. Marzani, and C. Daraio, "Engineered metabarrier as shield from seismic surface waves," Scientific Reports, vol. 6, no. 1, Dec. 2016.

[12]P. Cacciola and A. Tombari, "Vibrating barrier: a novel device for the passive control of structures under ground motion," Proceedings of the Royal Society of London A: Mathematical, Physical and Engineering Sciences, vol. 471, no. 2179, Jul. 2015.

[13]G. B. Warburton, J. D. Richardson, and J. J. Webster, "Forced Vibrations of Two Masses on an Elastic Half Space," Journal of Applied Mechanics, vol. 38, no. 1, p. 148, 1971.

[14]M. Lou, H. Wang, X. Chen, and Y. Zhai, "Structure–soil–structure interaction: Literature review," Soil Dynamics and Earthquake Engineering, vol. 31, no. 12, pp. 1724–1731, Dec. 2011.

[15]P. Cacciola, M. G. Espinosa, and A. Tombari, "Vibration control of piled-structures through structure-soil-structure-interaction," Soil Dynamics and Earthquake Engineering, vol. 77, pp. 47–57, Oct. 2015.

[16]A. Tombari, I. Zentner, and P. Cacciola, "Sensitivity of the stochastic response of structures coupled with vibrating barriers," Probabilistic Engineering Mechanics, vol. 44, pp. 183–193, Apr. 2016.

[17]P. Cacciola, N. Banjanac, and A. Tombari, "Vibration Control of an existing building through the Vibrating Barrier," Procedia Engineering, vol. 199, pp. 1598–1603, 2017.

[18]J. D. Coronado, R. Lomurno, A. Tombari, and P. Cacciola, "Improving Urban Seismic Resilience through Vibrating Barriers," in ICOSSAR 2017, Vienna, Austria, 2017.

[19]A. Tombari, M. Garcia Espinosa, N. A. Alexander, and P. Cacciola, "Vibration control of a cluster of buildings through the Vibrating Barrier," Mechanical Systems and Signal Processing, vol. 101, pp. 219–236, Feb. 2018.

[20]M. C. Smith, "Synthesis of mechanical networks: the inerter," IEEE Transactions on Automatic Control, vol. 47, no. 10, pp. 1648–1662, Oct. 2002.

[21]C. Papageorgiou and M. C. Smith, "Laboratory experimental testing of inerters," 2005, pp. 3351–3356.

[22] Zhao, C., J. Kikuchi, M. Ikenaga, K. Ikago and N. Inoue, 2016: Viscoelastically supported viscous mass damper incorporated into a seismic isolation system. *Journal of Earthquake and Tsunami*, 10, no. 3, 1640009.

[23]L. Marian and A. Giaralis, "Optimal design of a novel tuned mass-damper–inerter (TMDI) passive vibration control configuration for stochastically support-excited structural systems," Probabilistic Engineering Mechanics, vol. 38, pp. 156–164, Oct. 2014.

[24]L. Marian and A. Giaralis, "The tuned mass-damper-inerter for harmonic vibrations suppression, attached mass reduction, and energy harvesting," Smart Structures and Systems, vol. 19, no. 6, pp. 665–678, 2017.

[25]D. Pietrosanti, M. De Angelis, and M. Basili, "Optimal design and performance evaluation of systems with Tuned Mass Damper Inerter (TMDI): Optimal Design and Performance of Tuned Mass Damper Inerter Systems," Earthquake Engineering & Structural Dynamics, vol. 46, no. 8, pp. 1367–1388, Jul. 2017.

[26]I. F. Lazar, S. A. Neild, and D. J. Wagg, "Using an inerter-based device for structural vibration suppression: USING AN INERTER-BASED DEVICE FOR STRUCTURAL VIBRATION SUPPRESSION," Earthquake Engineering & Structural Dynamics, vol. 43, no. 8, pp. 1129–1147, Jul. 2014.

[27]A. Giaralis and A. A. Taflanidis, "Optimal tuned mass-damper-inerter (TMDI) design for seismically excited MDOF structures with model uncertainties based on reliability criteria," Structural Control and Health Monitoring, vol. 25, no. 2, p. e2082, Feb. 2018.

[28]D. De Domenico and G. Ricciardi, "An enhanced base isolation system equipped with optimal tuned mass damper inerter (TMDI): An enhanced base-isolation system equipped with optimal tuned mass damper inerter (TMDI)," Earthquake Engineering & Structural Dynamics, vol. 47, no. 5, pp. 1169–1192, Apr. 2018.

[29]N. Makris and G. Kampas, "Seismic Protection of Structures with Supplemental Rotational Inertia," Journal of Engineering Mechanics, vol. 142, no. 11, p. 04016089, Nov. 2016.

[30]J. S. Mulliken and D. L. Karabalis, "Discrete model for dynamic through-the-soil coupling of 3-D foundations and structures," Earthquake Engineering & Structural Dynamics, vol. 27, no. 7, pp. 687–710, Jul. 1998.

[31] Casciati F and Faravelli L, "Dynamic Transient Analysis of Systems with Material Nonlinearity: a Model Order Reduction Approach" Smart Structures and Systems, vol 18, no. 1. 2016.

[32]S. L. Kramer, Geotechnical earthquake engineering. Upper Saddle River, N.J.: Prentice Hall, 1996.

[33]L. Zuo, "Effective and Robust Vibration Control Using Series Multiple Tuned-Mass Dampers," Journal of Vibration and Acoustics, vol. 131, no. 3, p. 031003, 2009.

[34]R. Toscano, Structured controllers for uncertain systems: a stochastic optimization approach. London; New York: Springer, 2013.

[35]L. D. Lutes and S. Sarkani, Random vibrations [recurso electrónico] analysis of structural and mechanical systems. Paises Bajos; Estados Unidos: Elsevier, 2004.

[36]R. W. Clough and J. Penzien, Dynamics of structures. New York: McGraw-Hill, 1975.

[37] CEN Eurocode 8: Design of Structures for Earthquake Resistance - Part 1: General Rules, Seismic Actions and Rules for Buildings. EN 1998-1: 2003 E. Comité Européen de Normalisation, Brussels, 2004

[38]A. Giaralis and P. D. Spanos, "Derivation of response spectrum compatible non-stationary stochastic processes relying on Monte Carlo-based peak factor estimation," Earthquakes and Structures, vol. 3, no. 5, pp. 719–747, Sep. 2012.

[39]M. Shinozuka and G. Deodatis, "Simulation of Stochastic Processes by Spectral Representation," Applied Mechanics Reviews, vol. 44, no. 4, p. 191, 1991.

[40] PC Jennings, GW Housner, C.Tsai Simulated earthquake motions for design purpose. In: Proc 4th World conference earth. Engineering Santiago, A(1);p. 145–60, 1969

[41]P. Cacciola, L. D'Amico, and I. Zentner, "New insights in the analysis of the structural response to response-spectrum-compatible accelerograms," Engineering Structures, vol. 78, pp. 3–16, Nov. 2014.